Contents lists available at ScienceDirect

Digital Chinese Medicine

journal homepage: http://www.keaipublishing.com/dcmed

The modulating of Qingguang'an II Formula on gut microbiota in mice with chronic high intraocular pressure by 16S rDNA sequencing

ZHOU Yasha[a], GAO Wenyong[b], HUANG Yu[c], XIA Xin[c], XIAO Li[d], DENG Ying[d], PENG Qinghua[d], PENG Jun[c*]

a. School of Integrated Chinese and Western Medicine, Hunan University of Chinese Medicine, Changsha, Hunan 410208, China

b. Faculty of Biopharmaceutical, Ubon Ratchathani University, Warin Chamrap, Ubon Ratchathani 34190, Thailand

c. Department of Ophthalmology, The First Hospital of Hunan University of Chinese Medicine, Changsha, Hunan 410007, China

d. School of Chinese Medicine, Hunan University of Chinese Medicine, Changsha, Hunan 410208, China

ARTICLE INFO

Article history
Received 01 September 2024
Accepted 13 November 2024
Available online 25 December 2024

Keywords
Qingguang'an II Formula
Chronic high intraocular pressure
16S rDNA sequencing
Optic neuroprotection
Gut microbiota

ABSTRACT

Objective To investigate the effects of Qingguang'an II Formula (QGA II) on the gut microbiota of mice with chronic high intraocular pressure (IOP) model, and explore its key microbiota for protecting the optic nerve.

Methods A total of 10 specific pathogen free (SPF) grade female DBA/2J mice were randomly divided into model group and QGA II group (n = 5 for each group), while additional 5 SPF-grade female C57BL/6J mice were assigned to control group. Mice presented spontaneous high IOP and showed elevated approximately at the age of seven months. The high IOP was maintained until week 38, when gavage was initiated. Mice in control group underwent the same intragastric treatment, while those in QGA II group were gavaged with QGA II (9.67 g/kg), once a day for four weeks. Retinal morphology was examined using hematoxylin and eosin (HE) staining, with the number of retinal ganglion cells (RGCs) counted. The expression level of Brn3a protein, a specific marker for RGCs, was detected by immunofluorescence, with the mean optical density (OD) measured for quantitative analysis. In addition, 16S rDNA sequencing was leveraged to analyze changes in the diversity of gut microbiota, including their α-diversity (Chao1, Shannon, Pielou's evenness, and observed species index) and β-diversity. Venn diagrams and linear discriminant analysis effect size (LEfSe) analysis was employed to investigate the number of amplicon sequence variants (ASVs), the abundance of differential gut microbiota species, and the classification of species at both the phylum and genus levels within the three groups of mice.

Results HE staining revealed that compared with control group, model group showed significant reduction in the number of RGCs ($P < 0.01$), with intracellular vacuolar degeneration and nuclear pyknosis. After QGA II treatment, the number of RGCs was significantly increased compared with model group ($P < 0.01$), with notable improvements in intracellular vacuolar degeneration. Immunofluorescence analysis showed that the mean OD of Brn3a protein was significantly decreased in model group compared with control group ($P < 0.01$), while QGA II treatment significantly elevated its expression level ($P < 0.01$). Analysis of α-diversity showed that after QGA II intervention, the Chao1, Shannon, and Pielou's evenness indices were significantly increased ($P < 0.01$), and the observed species index was elevated ($P < 0.05$). β-Diversity analysis demonstrated distinct clustering among the three groups,

*Corresponding author: PENG Jun, E-mail: 154451101@qq.com.

Peer review under the responsibility of Hunan University of Chinese Medicine.

DOI: 10.1016/j.dcmed.2025.01.006

Citation: ZHOU YS, GAO WY, HUANG Y, et al. The modulating of Qingguang'an II Formula on gut microbiota in mice with chronic high intraocular pressure by 16S rDNA sequencing. Digital Chinese Medicine, 2024, 7(4): 332-342.

indicating relatively low similarity in bacterial community structures. ASV clustering identified a total of 14 061 ASVs across all groups, with 9 514 ASVs shared between model and QGA II groups. At the phylum level, the abundance of *Bacteroidetes* was significantly decreased in model group compared with control group ($P < 0.01$), while *Firmicutes* and the *Firmicutes*/*Bacteroidetes* (F/B) ratio were significantly increased ($P < 0.01$). QGA II treatment significantly reduced both *Firmicutes* abundance and the F/B ratio ($P < 0.01$). At the genus level, *Lactobacillus* was dominant across all groups, with its abundance significantly increased in model group ($P < 0.01$) and subsequently decreased following QGA II intervention ($P < 0.05$).

Conclusion QGA II restructured the gut microbiota of DBA/2J mice with chronic high IOP, bringing changes in their diversity and abundance of components. *Firmicutes*, *Bacteroidetes*, *Lactobacillus*, along with their associated microorganisms, are likely critical components of the gut microbiota that contribute to the optic neuroprotective effects of QGA II on chronic high IOP mice.

1 Introduction

The gut-brain axis, a bidirectional communication pathway between the gastrointestinal tract and central nervous system, is crucial to maintaining brain health [1]. The gut microbiota plays a significant role in influencing important processes associated with the formation of central nervous system degenerative diseases, including Parkinson's disease, Alzheimer's disease, and autism [2, 3]. It was reported that many retinal illnesses, as well, were closely linked to alterations in gut microbiota within human body, giving rise to the concept of the "gut-retina axis". For example, PENG [4] clarified that intestinal mucosal immune disorders caused damage to neurons in the inner retinal layer, followed by alterations in retinal visual function through the utilization of dextran sodium sulfate (DSS)-induced intestinal-retinal injury model. It is believed that retina-related disorders might be related to the activation of CD4+ T cells that are influenced by the gut microbiota. These cells would penetrate the eye after the blood-retinal barrier has been weakened by high intraocular pressure (IOP). CD4+ T cells in the eye interact with retinal ganglion cells (RGCs) that express heat shock protein (HSP), leading to a cross-reactivity. This process ultimately results in optic neurodegeneration, promoting the development of glaucoma [5]. A study observed a significant reduction in this cross-reactivity in a germ-free mice (i.e., mice without gastrointestinal bacteria), effectively inhibiting the T-cell response related to glaucoma and thus markedly suppressing the progression of the disease [6]. These findings have brought insights and laid a solid foundation to explore new treatment for glaucoma.

Glaucomatous optic neuropathy is a degenerative condition affecting the optic nerve. It is a leading cause of irreversible blindness, with no effective treatment available. Previous studies have demonstrated that Qingguang'an II Formula (QGA II) exerted a neuroprotective effect on the optic nerve in mouse models with chronic high IOP [7]. The protective effects were mediated through the regulation of the sirtuin 1 (SIRT1)/peroxisome proliferator-activated receptor gamma coactivator 1-alpha (PGC-1α) signaling pathway, upregulation of rat sarcoma virus (Ras), mitogen-activated protein kinase (MEK), and extracellular signal-regulated kinase (ERK) proteins, and inhibition of the ras homolog gene family, member A (Rho)/Rho-associated coiled-coil containing protein kinase (ROCK) signaling pathway, leading to a reduction in the apoptosis of RGCs [8-11]. These findings have highlighted the potential of QGA II as a promising novel therapeutic agent for the protection of the optic nerve. However, QGA II has quite complex components, whose metabolism and absorption can be markedly impacted by the gut microbiota within the body. Additionally, the formula, in return, plays a role in the regulation of the gut microbiota, contributing to the prevention and treatment of certain diseases. Given the inseparable relationship among the traditional Chinese medicine (TCM) formula, gut microbiota, and optic nerve protection, this study aimed to use 16S rDNA sequencing technology for investigating the modulatory effects of QGA II on the structure of gut microbiota in the DBA/2J mice with chronic high IOP, exploring underlying mechanisms of QGA II for the treatment of retinal diseases.

2 Materials and methods

2.1 Animals

In this study, a total of 10 specific pathogen free (SPF) grade female DBA/2J mice aged 8 weeks old were purchased from Beijing Vital River Laboratory Animal Technology Co., Ltd. (Beijing, China), with laboratory facility certificate No. SCXK (Jing) 2021-0006. Additional 5 SPF grade female C57BL/6J mice aged eight weeks old were purchased from Hunan Slake Jingda Experimental Animal Co., Ltd. (Changsha, China), with laboratory facility certificate No. SCXK (Xiang) 2019-0004. The mice were placed at a constant temperature of 22 ± 2 °C and a humidity of about 55% under a controlled 12 h light-dark

cycle, with free access to food and water. All experimental protocols were approved by the Animal Ethics Committee of Hunan University of Chinese Medicine (LL2021030202).

2.2 QGA II preparation

The QGA II comprising 15 g of Gouqizi (Lycii Fructus), 15 g of Huangqi (Astragali Radix), 10 g of Chuangxiong (Chuanxiong Rhizoma), 15 g of Nvzhenzi (Ligustri Lucidi Fructus), and 10 g of Niuxi (Achyranthis Bidentatae Radix) was purchased from The First Hospital of Hunan University of Chinese Medicine. Additionally, 10 g of Dengzhanxixin (Erigerontis Herba) were purchased from Kunming Daodi Prepared Slices of Chinese Crude Factory. After soaking in distilled water for 2 h, the herbs were decocted twice with water for 1 h each time, which was subsequently stored at 4 °C.

2.3 Reagents and chemicals

Anti-Brn3a antibodies were acquired from Abcam Plc (UK). Goat anti-rabbit immunoglobulin G (IgG) was obtained from Wuhan Servicebio Technology Co., Ltd. (China). Quant-iT PicoGreen dsDNA assay kit, Agarose, and Agilent high-sensitivity DNA kit were obtained from Invitrogen Corporation (USA). Mag-Bind soil DNA kit was purchased from Sigma Aldrich Co., Ltd. (USA). MiSeq reagent kit V3 and TruSeq Nano DNA LT library prep kit were acquired from Illumina, Inc. (USA).

2.4 Instruments

Rebound tonometer (Tiolatoy, Icare), polymerase chain reaction (PCR) amplifier (ABI, 2720), electrophoresis apparatus (Beijing Liuyi Biotechnology Co., Ltd., DYY-6C), gel imaging system (Beijing Baijing Biology Technology Co., Ltd., BG-GDS AUTO), NanoDrop (Thermo Scientific, NC2000), and upright optical microscope (Nikon Corporation, Nikon Eclipse E100).

2.5 Drug administration

The DBA/2J mice were utilized as models for studying chronic high IOP, a spontaneous disease progressively developed in the mice around seven months of age [12, 13]. Since then, the IOP was measured monthly from week 10 to 38 of age. According to prior research, mice with an IOP exceeding 21 mmHg at week 38 of age were deemed to have successfully established the model [10]. Ultimately, 10 DBA/2J mice meeting the criteria for model screening were included in the study. The mice were randomly assigned to model and QGA II groups (n = 5 for each group) using a random number table. An additional 5 C57BL/6J mice were designated as control group. Mice in control and model groups received 12.91 mL/(kg·d) of distilled water via intragastric administration, while those in the QGA II group were intragastrically given 9.67 g/(kg·d) of QGA II herbal liquid [10]. All mice were dosed daily for 4 weeks. These mice were subsequently anesthetized by intraperitoneal injection of 1% pentobarbital (0.2 mL/kg), followed by euthanasia via cervical dislocation. The left eyes of the mice in the three groups were harvested and placed in Eppendorf (EP) tubes containing fixative solution at room temperature for subsequent hematoxylin and eosin (HE) staining and immunofluorescence. Their colons were excised under sterile conditions using a sterile scalpel to collect the fecal matter, which was swiftly frozen in liquid nitrogen and immediately transferred into a freezer of – 80 °C for gut microbiota analysis.

2.6 Examination of the morphology of the retina by HE staining

The eyeball tissues were fixed in an eye fixative fluid for 48 h. Subsequently, the samples were dehydrated through a graded series of ethanol, specifically 75%, 85%, and 95%. The dehydrated samples were rinsed in xylene and then embedded with paraffin wax. Next, the samples were cut into 5 μm in thickness with the use of a microtome. The sections were then mounted onto glass slides, which were later placed in xylene to remove the paraffin wax. After removal, the sections were rehydrated using a decreasingly graded series of ethanol, and the gradients were 100%, 95%, and 75%, respectively. After that, the samples were stained using HE for 5 min, and then rinsed using running water to wash off the excessive HE. The next step was to differentiate the stained samples in a solution of acid alcohol (1% hydrochloric acid in 70% ethanol) for 20 s, and rinsed again under running water, followed by being blued in alkaline water, and stained again using HE for 2 min. The stained samples were dehydrated once more with the use of 100% ethanol. The samples were then cleared in xylene and mounted with a suitable mounting medium. Lastly, dry samples were placed under a light microscope for examination, during which process the number of RGCs within each slide was recorded.

2.7 Detection of Brn3a proteins in the retina using immunofluorescence technology

The paraffin sections were subjected to antigen retrieval in a water bath following deparaffinization. The sections were then blocked with 5% goat serum, followed by 40 – 50 μL of anti-Brn3a antibody (diluting ratio of 1 : 2 000), and were covered with wet box overnight at 4 °C. Subsequently, the slides were washed with PBS for three times, 5 min each time. The secondary antibody (diluting ratio of 1 : 500) was added and incubated for 50 min at room temperature, and the slides were washed with phosphate

buffered saline (PBS) for three times, 5 min per time. The slides were slightly dried and incubated with tyramide signal amplification (TSA) dropwise and shielded from light for 10 min at room temperature. After incubation, the slides were placed in tris-buffered saline Tween-20 (TBST), followed by PBS rinsing for three times. The nuclei were counterstained with 4',6-diamidino-2-phenylindole (DAPI) solution for 10 min at room temperature, after which autofluorescence was effectively quenched. The mean optical density (OD) values were analyzed using ImageJ software.

2.8 DNA extraction and polymerase chain reaction (PCR) amplification of gut microbiota

The stool samples were transferred into sterile microcentrifuge tubes containing an extraction lysis buffer and homogenized. Nucleic acids were then extracted using MagBind soil DNA kit, and the resulting DNA was quantified. The quality of the DNA extraction was assessed by running a 0.8% agarose gel electrophoresis. Bacterial DNA fragments of approximately 480 bp in length were selected for analysis. PCR amplification was performed using specific primers targeting the V3 – V4 region of bacterial 16S rRNA sequencing: 338F (5'-ACTCCTACGGGAGGCAGCA-3') and 806R (5'-GGACTACHVGGGTWTCTAAT-3'). The amplified products were purified and recovered using magnetic bead technology for subsequent fluorescence quantification. Based on the quantification results, the samples were then fixed in the required proportions to satisfy the sequencing requirements for each individual sample. To calculate the mixing proportions, the required volume of each sample based on its concentration and target sequencing amount was determined, then combined in the appropriate ratios to reach the target total volume. To ensure representativeness in the mixed samples, samples from all groups were included in a balanced proportion based on their microbial abundance, and technical replicates were performed to ensure consistency and adequate coverage within the mixed samples.

2.9 Preparation of sequencing libraries and quality control

Sequencing libraries were prepared using the Illumina MiSeq/NovaSeq sequencing platform. A 1 μL aliquot of each library was assessed for quality, with the expectation that qualified libraries would show a distinct peak, be free of adapters, and have concentrations exceeding 2 nmol/L as determined by Quant iT PicoGreen dsDNA assay kit on a Promega Quantifluor Fluorescence Quantification System. Libraries that met these criteria were then sequenced using the paired-end sequencing on the Illumina MiSeq/NovaSeq platform to analyze the DNA fragments.

2.10 Analysis of species information in gut microbiota

Following the initial decoding of raw sequence data, the sequences were processed using the Divisive Amplicon Denoising Algorithm 2 (DADA2) plugin, which involved steps such as primer trimming, quality filtering, denoising, merging, and the removal of chimeric sequences. The sequences were subsequently clustered based on their similarity to generate amplicon sequence variants (ASVs) and compile the corresponding abundance data.

The α-diversity and β-diversity indices were calculated to evaluate the intra-sample diversity and inter-sample variations in microbial community structure among different groups. In the α-diversity indices, species richness was quantified using the Chao1 and observed species index, diversity was measured by the Shannon index, and evenness was assessed with Pielou's evenness index. Species annotation was performed using the Greengenes database. The QIIME2 V2019.4 classification framework, employing the classify-sklearn algorithm, was applied to each ASV feature sequence. Default parameters were utilized within the QIIME2 software, and a pre-trained Naive Bayes classifier was employed to obtain species annotation information. Taxonomic classification of ASVs identified differentially abundant taxa across six taxonomic levels: phylum, class, order, family, genus, and species.

2.11 Statistical analysis

Measurement data were presented as mean ± standard deviation (SD) and analyzed using SPSS 25.0. Tests for normality and homogeneity of variance were initially conducted. If the data conformed to the assumptions of normality and homogeneity of variance, multiple group comparisons were performed using analysis of variance (ANOVA). If these assumptions were violated, non-parametric tests were used for multiple group comparisons. $P < 0.05$ was considered statistically significant, and $P < 0.01$ was regarded the presence of highly statistically significant difference. Relative abundance bar plots and Venn diagrams were generated using R scripts or GraphPad Prism. Differential marker species among groups were identified through linear discriminant analysis effect size (LEfSe) analysis using the Python LEfSe package in conjunction with R packages ggtree and ggplot2 for visualization and statistical processing.

3 Results

3.1 IOP of mice in each group

The IOP of C57BL/6J mice remained relatively stable, fluctuating between 10 and 16 mmHg from week 10 to week 38 of age. In DBA/2J mice, IOP increased to beyond 21 mmHg after 30 weeks. The IOP of DBA/2J mice was

higher than that of C57BL/6J mice starting at week 14 ($P < 0.05$). The IOP of DBA/2J mice was significantly higher than that of C57BL/6J mice starting at week 18 ($P < 0.01$). A comparison of IOP between DBA/2J and C57BL/6J mice at different time points from week 10 to week 38 of age is shown in Figure 1.

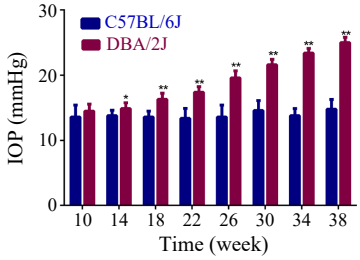

Figure 1 IOP values in mice from week 10 to week 38 of age

$^{*}P < 0.05$ and $^{**}P < 0.01$, compared with C57BL/6J mice.

3.2 Changes in the retinal structure of mice in different groups by HE staining

In control group, light microscopy revealed clear and intact retinal layers, with RGCs of a round or oval shape arranged in a single layer (Figure 2A). However, the model group showed a decrease in RGCs and nerve fiber breakage in ganglion cell layer (GCL) (Figure 2B, with yellow arrow). In QGA II group, there were more RGCs and fewer nerve fiber ruptures than model group (Figure 2C). The model group exhibited a significant reduction in the number of RGCs, compared with control group (Figure 2D, $P < 0.01$). In QGA II group, the number of RGCs was higher than model group (Figure 2D, $P < 0.01$).

3.3 Detection of the expression level of Brn3a protein in the retina by immunofluorescence

According to the results of immunofluorescence labeling, Brn3a was expressed at high level in the GCL of control group. However, in model group, the expression level of Brn3a was significantly decreased in the GCL. The use of QGA II was found to enhance the expression of Brn3a in the GCL of DBA/2J mice (Figure 3). Additionally, the mean OD values of Brn3a proteins were significantly reduced in model group compared with control group ($P < 0.01$). Compared with model group, QGA II group showed significantly increased OD values for Brn3a protein ($P < 0.01$).

3.4 Analysis of α-diversity indices

Figures 4A – 4D illustrate the rarefaction curves for the α-diversity indices, including Chao 1, Shannon, Pielou's evenness, and observed species. These curves show that as the number of reads increases, the richness, diversity, evenness, and coverage indices reach a plateau. This

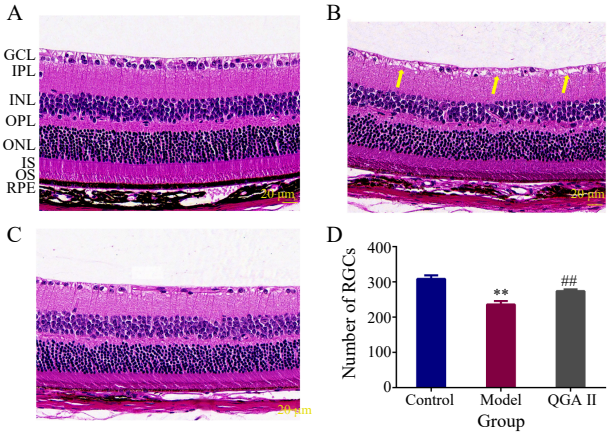

Figure 2 Effects of QGA II on retinal morphology and RGC counts in mice (× 400)

A, control group. B, model group. C, QGA II group. D, the number of RGCs. GCL, ganglion cell layer. IPL, inner plexiform layer. INL, inner nuclear layer. OPL, outer plexiform layer. ONL, outer nuclear layer. IS, inner segment of photoreceptors. OS, outer segment of photoreceptors. RPE, retinal pigment epithelium. RGCs, retinal ganglion cells. Data were represented as mean ± SD. $^{**}P < 0.01$, compared with control group. $^{\#\#}P < 0.01$, compared with model group.

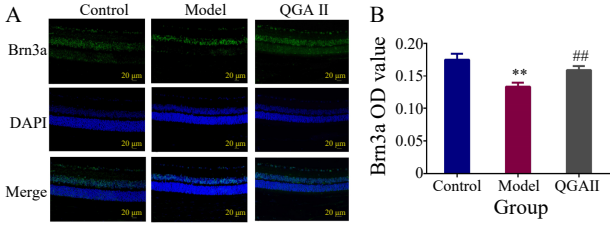

Figure 3 Effects of QGA II on Brn3a protein expression in DBA/2J mice

A, immunofluorescence-labeled localized Brn3a protein in mice (× 400). B, the OD value of Brn3a protein in the retina. Data were represented as mean ± SD. $^{**}P < 0.01$, compared with control group. $^{\#\#}P < 0.01$, compared with model group.

finding suggested the presence of adequate sequencing depth, which ensured that the sequencing process was both appropriate and statistically significant.

The α-diversity analysis revealed that model group exhibited decreased bacterial richness, diversity, evenness, and coverage compared with control group, but the differences were not statistically significant ($P > 0.05$). Compared with model group, QGA II group demonstrated markedly elevated Chao 1, Shannon, Pielou's evenness indices ($P < 0.01$), and observed species indices ($P < 0.05$). The detailed results are presented in Figure 4E – 4H, and Table 1.

3.5 Analysis of β-diversity indices

Based on Bray-Curtis distances, the principal coordinate analysis (PCoA) of gut microbiota among groups is demonstrated in Figure 5A. The analysis showed that Axis 1, which accounted for 19.5% of the variance, was the main

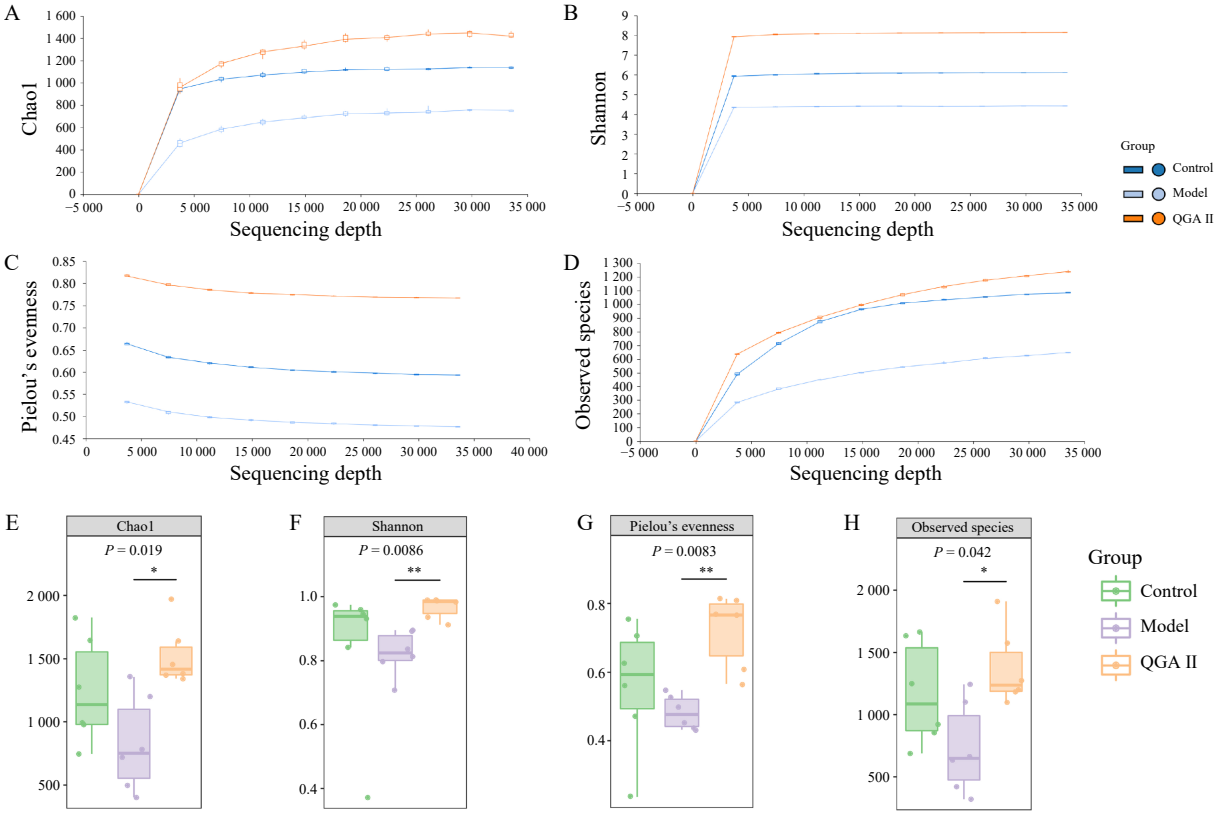

Figure 4 Effects of QGA II on α-diversity indices

A – D, rarefaction curve of Chao 1, Shannon, Pielou's evenness, and observed species indices of mice in the three groups, respectively. E – H, box plots of Chao 1, Shannon, Pielou's evenness, and observed species indices of mice in the three groups, respectively. $^{*}P < 0.05$ and $^{**}P < 0.01$, compared with model group.

Table 1 Comparison of the α-diversity index of gut microbiota of mice in each group

Group	Chao 1	Shannon	Pielou's evenness	Observed species
Control	1 244.42 ± 420.48	5.73 ± 2.10	0.56 ± 0.19	1 168.95 ± 414.86
Model	827.08 ± 379.70	4.53 ± 0.72	0.48 ± 0.05	730.48 ± 368.36
QGA II	1 526.09 ± 241.48*	7.50 ± 1.15**	0.72 ± 0.11**	1 374.68 ± 309.70*

$^{*}P < 0.05$ and $^{**}P < 0.01$, compared with model group.

contributor to sample differentiation, followed by Axis 2, which explained 13.9% of the variance. According to Bray-Curtis distances, the non-metric multidimensional scaling (NMDS) of gut microbiota among the groups is illustrated in Figure 5B. The analysis revealed that samples from control, model, and QGA II groups were discernible, indicating a relatively low similarity in the structure of bacterial community among the three groups.

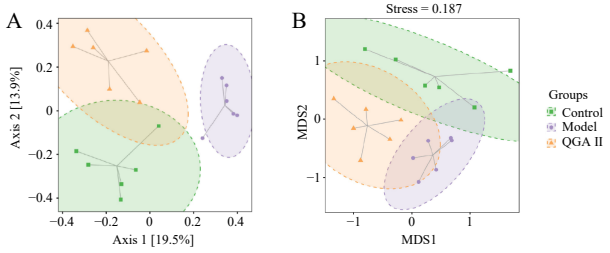

Figure 5 Analysis of β-diversity indices based on PCoA and NMDS

A, Bray-Curtis distance-based PCoA. B, Bray-Curtis distance-based NMDS. The elliptical dashed circles in the figure represent 95% confidence ellipses.

3.6 Distribution and differences in the composition of the gut microbiota at the phylum level

The structure of gut microbiota in different mice was investigated at the phylum level. A bar plot depicting the top 20 phylum by relative abundance is illustrated in Figure 6A. The dominant flora included *Firmicutes*, *Bacteroidetes*, *Proteobacteria*, *Saccharibacteria* (*TM7*), and *Actinobacteria*.

A comparative analysis of relative abundance of bacteria among the groups revealed that model group exhibited a significant decrease in *Bacteroidetes* compared with control group (Figure 6B, $P < 0.01$). Following intervention with QGA II, there was an increase in its relative abundance, although this change was not statistically

significant (Figure 6B, $P > 0.05$). Moreover, compared with control group, model group showed a significant increase in *Firmicutes* abundance and *Firmicutes*/*Bacteroidetes* (F/B) ratio (Figure 6B and 6C, $P < 0.01$). After QGA II intervention, a significant decrease in their relative abundance was observed ($P < 0.01$). Conversely, although model group showed a slight decrease in the relative abundance of *Proteobacteria* compared with control group, this difference was not statistically significant (Figure 6B, $P > 0.05$). However, after intervention with QGA II, a significant increase in relative abundance was observed (Figure 6B, $P < 0.01$).

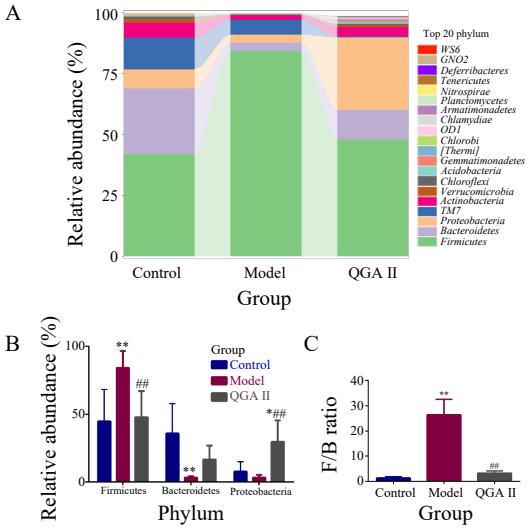

Figure 6 Distribution and differences in the composition of the gut microbiota at the phylum level in each group

A, relative abundance of gut microbiota at the phylum level. B, the top 3 species in terms of relative abundance at the phylum level. C, F/B ratio. Data were represented as mean ± SD. $^{*}P < 0.05$ and $^{**}P < 0.01$, compared with control group. $^{\#\#}P < 0.01$, compared with model group.

3.7 Distribution and differences in the composition of the gut microbiota at the genus level

At the genus level, a bar plot illustrating the relative abundance of the top 20 genus is depicted in Figure 7A. These predominant genera include *Lactobacillus*, *Desulfovibrio*, *Allobaculum*, *Ochrobactrum*, and *Delftia*, with *Lactobacillus* being the predominant genus. A comparative analysis revealed a significant increase in the relative abundance of *Lactobacillus* in model group compared with control group (Figure 7B, $P < 0.01$). Following intervention with QGA II, there was a significant decrease in its relative abundance (Figure 7B, $P < 0.05$).

3.8 ASVs Venn diagram and analysis

Figure 8A shows the number of ASVs in the three groups. Control, model, and QGA II groups were collectively

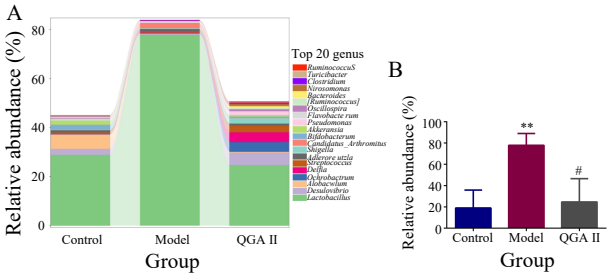

Figure 7 Distribution and differences in the composition of the gut microbiota at the genus level in each group

A, relative abundance of the gut microbiota at the genus level. B, relative abundance of *Lactobacillus*. Data were represented as mean ± SD. $^{**}P < 0.01$, compared with control group. $^{\#}P < 0.05$, compared with model group.

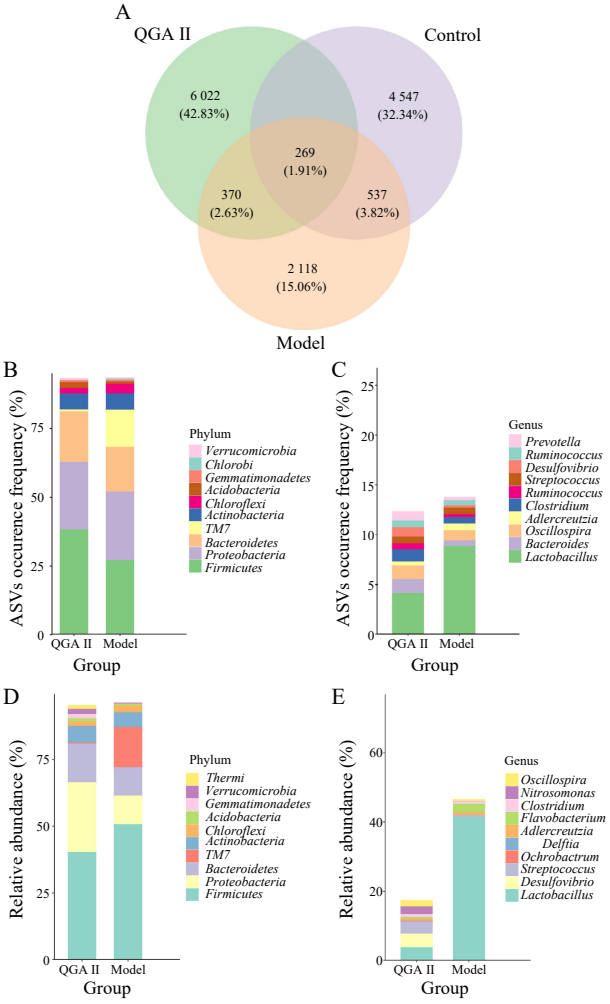

Figure 8 ASVs analysis and taxonomic composition among the groups

A, Venn diagram of ASVs of the gut microbiota in the three groups. B and C, frequency distribution of bacterial taxa at phylum and genus levels in different Venn diagram regions, respectively. D and E, relative abundance of bacterial taxa at phylum and genus levels in different Venn diagram regions, respectively. Different colors represent distinct taxonomic groups, and the percentage on each axis indicates the proportion of corresponding bacterial taxa.

clustered into a total of 14 061 ASVs. The sequences from model group and QGA II group were clustered into 9 514 ASVs. Within this clustering, 27.91% were unique to model group, while 65.38% were unique to QGA II group. This finding indicated increase in microbial diversity in the mice following gavage with QGA II.

In terms of species frequency, at the phylum level, QGA II group showed a decrease in *TM7* and an increase in *Proteobacteria*, *Firmicutes*, and *Bacteroidetes*, compared with model group (Figure 8B). At the genus level, relative to model group, QGA II group demonstrated a reduction in *Lactobacillus* and *Adlercreutzia*, accompanied by an increase in *Bacteroides*, *Oscillospira*, and *Clostridium* (Figure 8C). Regarding relative abundance of the species, at the phylum level, QGA II group demonstrated a decrease in *Firmicutes* and *TM7*, and an increase in *Bacteroidetes* and *Actinobacteria* compared with model group (Figure 8D). At the genus level, QGA II group exhibited a reduction in *Lactobacillus* and an elevation in *Desulfovibrio* and *Streptococcus* compared with model group (Figure 8E).

3.9 LEfSe analysis

Using the LEfSe analysis method (LDA > 2), a comparative analysis was conducted to identify gut microbiota taxa with statistically significant differences among control, model, and QGA II groups (Figure 9). It was revealed that QGA II group exhibited a more diverse microbiota profile. Specifically, model group showed a higher relative abundance in eight taxa, including the genus *Lactobacillus*, *Lactobacillaceae*, *Lactobacillales*, and *Firmicutes*. In contrast, QGA II group demonstrated an increased relative abundance in 133 taxa, including the *Proteobacteria*, *Alphaproteobacteria*, *Bacteroidetes*, *Bacteroidales*, and *Bacteroidia*.

4 Discussion

4.1 Syndromes closely related to optic neuropathy caused by chronic high IOP

This study demonstrated that the DBA/2J mice in QGA II group exhibited mitigated retinal damage and significantly increased expression level of Brn3a protein, a common marker for the detection of RGCs [14, 15], compared with mice in model group, indicating that QGA II did exert a protective effect on the optic nerve. “Chronic” in the name of the investigated diseases refers to a prolonged disease course leading to Qi depletion and Yin damage, resulting in a state of “deficiency”. The liver and kidneys, which were affected most by the depletion of Qi and Yin, bear primary consequences from the “deficiency” associated with chronic high IOP. Therefore, clinical treatment for the “deficiency” focuses on “tonification”, particularly

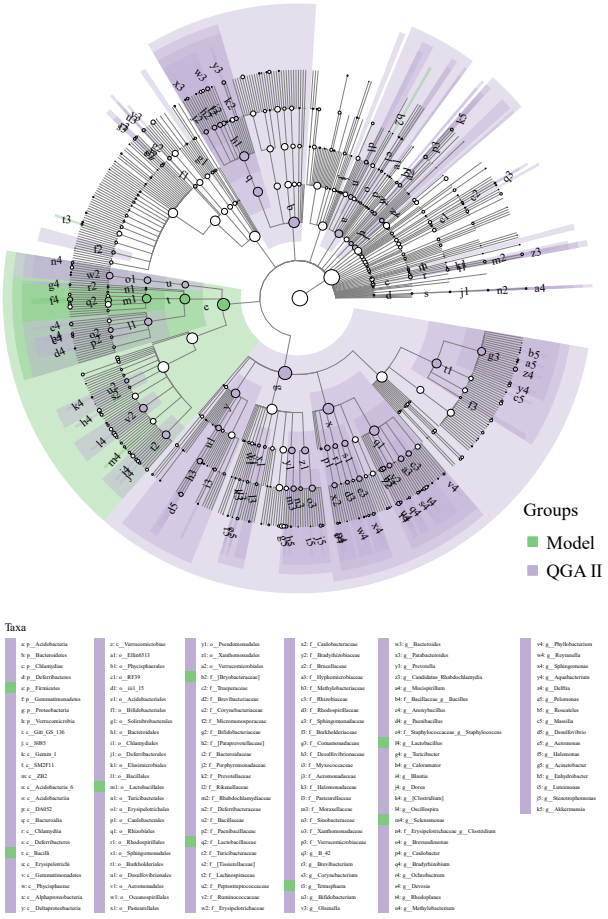

Figure 9 Taxonomic hierarohy and differential abundance analysis among the groups

The inner to outer circles respectively showed the taxonomic rank relationships of the major taxonomic units from phylum to genus. Node size corresponded to the mean relative abundance of that taxonomic unit. Hollow nodes represented taxonomic units with insignificant, whereas nodes of colors indicated that these taxonomic units reflected significant inter-group differences and were more abundant in the group represented by that color.

nourishing the liver and kidneys. High IOP is commonly due to the poor drainage of ocular contents, primarily in the aqueous humor, leading to a state of “blood stasis”.

Taking this pathogenesis into consideration QGA II incorporates Huangqi (Astragali Radix) to address the underlying deficiencies and prominently features Gouqizi (Lycii Fructus), Nvzhenzi (Ligustri Lucidi Fructus), and Niuxi (Achyranthis Bidentatae Radix) to nourish and support liver and kidney functions. The stagnation of aqueous humor and obstruction of ocular pathways, which contribute to poor circulation, can be addressed using this formula as well. Therefore, the formula included Niuxi (Achyranthis Bidentatae Radix) and Dengzhanxixin (Erigerontis Herba) to invigorate blood flow, and Chuangxiong (Chuanxiong Rhizoma) to promote Qi movement, aiming to resolve the stasis in the underlying mechanism of high IOP. In this experiment, DBA/2J mice began to show elevated IOP at the age of 7 months old,

which peaked around 9 to 10 months old [16, 17], and experienced persistent aqueous humor outflow obstruction, corresponding to the stasis described in TCM. Moreover, these mice exhibited age-related progressive retinal degeneration [17], aligning with the deficiencies presented in many chronic conditions. Therefore, the pathogenic features presented by the DBA/2J mice were consistent with the syndrome of Qi and Yin deficiencies and pulse-obstructing blood stasis caused by chronic high IOP.

4.2 Influences of QGA II on gut microbiota of mice with optic neuropathy caused by chronic high IOP

Microbiomics offered a comprehensive understanding of the total gene sequences within the gut microbiota. The TCM compound QGA II exemplified a drug phenotypic profile, and the investigation of its effects on gut microbiota represented a specific application within the phenomics research of TCM. This study investigated the protective effects of QGA II on key components of the gut microbiota in mice with chronic high IOP, by examining their biodiversity using α-diversity indicies to thoroughly analyzing richness using Chao1 and observed species, microbial diversity using Shannon index, and uniformity using Pielou's evenness in the gut microbiota. Our findings demonstrated a significant reduction in both the richness and diversity of the gut microbiota in DBA/2J mice. However, intervention with QGA II notably restored and enhanced the richness and diversity of the gut microbiota while also modified its structural compositions. Analysis of β-diversity indices further corroborated these results, showing that QGA II treatment improved both microbial diversity and richness.

The association between glaucoma and gut microbiota was initially proposed by KOUNTOURAS et al. [18] in 2000, who hypothesized that *Helicobacter pylori* might contribute to the pathogenesis of glaucoma. Numerous studies subsequently investigated the interplay between microbial communities and the development of glaucoma. A study [19] utilizing glaucoma rat models reported a notable increase in the F/B ratio compared with control rats. In addition, the examination of gut microbiota in human patients with glaucoma has revealed a greater ratio of *Firmicutes* to *Bacteroidetes* in comparison with healthy individuals with open-angle glaucoma [20]. These findings have suggested a significant resemblance between alterations in gut microbiota observed in glaucoma rats and those found in human patients. *Firmicutes* and *Bacteroidetes* were the two dominant phyla in gut microbiota. Our research on DBA/2J mice revealed an elevated F/B ratio. However, QGA II treatment resulted in a reduction in the relative abundance of *Firmicutes* while an elevation in *Bacteroidetes*, thereby decreasing the F/B ratio. *Bacteroidetes*, particularly its constituent microbial populations, were recognized as key producers of short-chain fatty acids (SCFAs), which were essential for regulating the immune functions of the gut [21]. It was assumed that the chronic and episodic aggravation found in neurodegenerative disorders may be caused by an imbalance in the relative abundance among diverse bacterial populations rather than the presence of specific pathogenic bacteria. The modulation of the F/B ratio by QGA II may thus have exerted a critical mechanism underlying its protective effects on the optic nerve in DBA/2J mice.

Our study found that, at the genus level, DBA/2J mice exhibited a significant increase in the relative abundance of *Lactobacillus* and a significant decrease in *Bacteroides* compared with control group. In TCM, gut microbiota is conceptually associated with the spleen system, performing analogous functions. The spleen is crucial for vital energy (immunity), synthesis and distribution of essence and blood (microcirculation), and the aging process. Thus, TCM addresses glaucoma using a spleen-centric approach [22]. QGA II included Huangqi (Astragali Radix), a traditional herb renowned for its spleen-strengthening properties, which contribute to the restructure of the composition of gut microbiota. Additionally, Huangqi (Astragali Radix) and Gouqizi (Lycii Fructus) were rich in the polysaccharides in this formula. Due to their complex structures, polysaccharides are resistant to direct enzymatic degradation in the human digestive system and thus traverse to the large intestine. Therefore, gut microbiota play a pivotal role in the metabolism of polysaccharides, providing essential energy to the host, promoting the proliferation of beneficial bacteria, and supporting the maintenance of a balanced and healthy intestinal environment [23]. *Lactobacillus* is the most prevalent genus in gut microbiota [24] and a key representative of beneficial intestinal bacteria. LIU et al. [25] found that *Astragalus* polysaccharides significantly improved the structure of gut microbiota in osteoporosis rat models, with *Lactobacillus* emerging as a potentially crucial bacterial genus. Moreover, studies have concluded that Chuangxiong (Chuanxiong Rhizoma) and Nvzhenzi (Ligustri Lucidi Fructus) ameliorate pathological conditions by modulating the population of *Lactobacillus* in both human and animal models [26, 27]. In our study, the relative abundance of *Lactobacillus* was markedly elevated. The increase was thought to be associated with a decrease in overall diversity and richness of the gut microbiota in mouse models, leading to a disruption of microbial balance and a consequent rise in the relative abundance of *Lactobacillus*. Following intervention with QGA II, there was an observed increase in the diversity of gut microbiota, with microbial proportions gradually returning to a balanced state, reflected by a decrease in the abundance of *Lactobacillus*.

4.3 Significance and limitations of the study

This study had identified the impact of QGA II on gut microbiota of DBA/2J mice. The interaction with the gut microbiota maybe the mechanism by which the formula exerted its optic neuroprotective effects. However, this study had not yet explored the inherent relationships between gut microbiota and optic nerve alterations, which deserves further research in the future.

5 Conclusion

Our results demonstrate the effects of QGA II on the morphology of the retina and the structures of the gut microbiota in DBA/2J mice, offering insight into the exploration of associations between alterations in the gut microbial profile and the neuroprotective effects of TCM. QGA II may serve as a potential prebiotic agent to target the gut-eye axis for optic neuroprotection in chronic high IOP.

Fundings

National Natural Science Foundation of China (81904260), Scientific Research Project of Hunan Province Department of Education (22B0398), and Scientific Research Project of Traditional Chinese Medicine of Hunan Province (D2022045).

Competing interests

The authors declare no conflict of interest.

References

[1] KIM Y, LIM J, OH J. Taming neuroinflammation in Alzheimer's disease: the protective role of phytochemicals through the gut-brain axis. Biomedicine & Pharmacotherapy, 2024, 178: 117277.

[2] CRYAN JF, O'RIORDAN KJ, COWAN CSM, et al. The microbiota-gut-brain axis. Physiological Reviews, 2019, 99(4): 1877–2013.

[3] QUIGLEY EMM. Microbiota-brain-gut axis and neurodegenerative diseases. Current Neurology and Neuroscience Reports, 2017, 17(12): 94.

[4] PENG K. Research on regulatory mechanisms of the steap protein family on macrophages in gut retina axis. Chengdu: University of Electronic Science and Technology of China, 2020.

[5] XUE W, LI JJ, ZOU YL, et al. Microbiota and ocular diseases. Frontiers in Cellular and Infection Microbiology, 2021, 11: 759333.

[6] HERNÁNDEZ-ZULUETA J, BOLAÑOS-CHANG AJ, SANTA CRUZ-PAVLOVICH FJ, et al. Microbial dynamics in ophthalmic health: exploring the interplay between human microbiota and glaucoma pathogenesis. Medicina, 2024, 60(4): 592.

[7] JIANG PF, ZENG ZC, LIU DH, et al. Study on the safety of Qingguang'an II formula and its protectivemechanism on the optic nerve of chronic hypertension rats. China Journal of Traditional Chinese Medicine and Pharmacy, 2023, 38(5): 2010–2015.

[8] LV Y, JIANG PF, PENG J, et al. Protective effects of Qingguang'an II formula on the optic nerve based on network pharmacology and SIRT1/PGC-1α signaling pathway. Journal of Hunan University of Chinese Medicine, 2024, 44(8): 1438–1447.

[9] ZENG ZC, LI YX, QIN HY, et al. Protective effects and mechanism of active components of Qingguang'an II formula on retinal ganglion cells in DBA/2J mice with chronic intraocular hypertension. Journal of Hunan University of Chinese Medicine, 2022, 42(12): 1973–1981.

[10] SHI J, PENG J, YAO X, et al. Effect of Qingguang'an II on Rho/ROCK associated factors in the retina of DBA/2J mice. Journal of Hainan Medical University, 2022, 8(13): 16–21.

[11] QIN HY, ZENG ZC, LI YX, et al. Effect of Qingguang'an II decoction and its effective componentson the expression of Ras, MEK and ERK proteins in retina of DBA/2J mice. Journal of Hunan University of Chinese Medicine, 2022, 42(5): 738–742.

[12] YANG F, WU LL, GUO XJ, et al. Ocular findings and histological change in glaucoma model of DBA/2J mice. Chinese Journal of Experimental Ophthalmology, 2010, 28(2): 103–108.

[13] WANG J, DONG Y. Characterization of intraocular pressure pattern and changes of retinal ganglion cells in DBA2J glaucoma mice. International Journal of Ophthalmology, 2016, 9(2): 211–217.

[14] NADAL-NICOLÁS FM, GALINDO-ROMERO C, LUCAS-RUIZ F, et al. Pan-retinal ganglion cell markers in mice, rats, and rhesus macaques. Zoological Research, 2023, 44(1): 226–248.

[15] MENG M, CHAQOUR B, O'NEILL N, et al. Comparison of Brn3a and RBPMS labeling to assess retinal ganglion cell loss during aging and in a model of optic neuropathy. Investigative Ophthalmology & Visual Science, 2024, 65(4): 19.

[16] BIERLEIN ER, SMITH JC, VAN HOOK MJ. Mechanism for altered dark-adapted electroretinogram responses in DBA/2J mice includes pupil dilation deficits. Current Eye Research, 2022, 47(6): 897–907.

[17] CROSBIE DE, KEANEY J, TAM LCS, et al. Age-related changes in eye morphology and aqueous humor dynamics in DBA/2J mice using contrast-enhanced ocular MRI. Magnetic Resonance Imaging, 2019, 59: 10–16.

[18] KOUNTOURAS J, MYLOPOULOS N, BOURA P, et al. Relationship between *Helicobacter pylori* infection and glaucoma. Ophthalmology, 2001, 108(3): 599–604.

[19] ZHANG YL, ZHOU XJ, LU Y. Gut microbiota and derived metabolomic profiling in glaucoma with progressive neurodegeneration. Frontiers in Cellular and Infection Microbiology, 2022, 12: 968992.

[20] CHEN JL, CHEN DF, CHO KS. The role of gut microbiota in glaucoma progression and other retinal diseases. The American Journal of Pathology, 2023, 193(11): 1662–1668.

[21] ROSSER EC, PIPER CJM, MATEI DE, et al. Microbiota-derived metabolites suppress arthritis by amplifying aryl-hydrocarbon receptor activation in regulatory B cells. Cell Metabolism, 2020, 31(4): 837–851.

[22] LV Y, JIANG PF, LIU P, et al. Discussion on treatment of glaucoma from the spleen based onthe intestinal microflora. China Journal of Traditional Chinese Medicine and Pharmacy, 2022, 37(10): 5721–5725.

[23] ZHANG KL, LV M, HUN JY, et al. A review of studies on spleen deficiency syndrome based onIntestinal microflora. Modernization of Traditional Chinese Medicine and Materia

Medica-World Science and Technology, 2024, 26(3): 628–633.
[24] WAN YY. The mechanism study of jinteng qingbi granulesin the treatment of rheumatoid arthritis based on multi-omics. Suzhou: University of China Academy of Chinese Medical Sciences, 2023.
[25] LIU JS, LIU J, LIU L, et al. The gut microbiota alteration and the key bacteria in *Astragalus* polysaccharides (APS)-improved osteoporosis. Food Research International, 2020, 138: 109811.
[26] CHEN KZ, YU DD. Research progress on regulating gut microbiota with single traditional Chinese medicine for the prevention and treatment of postmenopausal osteoporosis. Xinjiang Journal of Traditional Chinese Medicine, 2023, 41(2): 87–90.
[27] ZHAO X, CHEN Y, LI L, et al. Effect of DLT-SML on chronic stable angina through ameliorating inflammation, correcting dyslipidemia, and regulating gut microbiota. Journal of Cardiovascular Pharmacology, 2021, 77(4): 458–469.

基于 16S rDNA 测序探讨青光安 II 号方对慢性高眼压模型小鼠肠道菌群的影响

周亚莎[a], GAO Wenyong[b], 黄雨[c], 夏鑫[c], 肖莉[d], 邓颖[d], 彭清华[d], 彭俊[c*]

a. 湖南中医药大学中西医结合学院, 湖南 长沙 410208, 中国
b. Faculty of Biopharmaceutical, Ubon Ratchathani University, Warin Chamrap, Ubon Ratchathani 34190, Thailand
c. 湖南中医药大学第一附属医院眼科, 湖南 长沙 410007, 中国
d. 湖南中医药大学中医学院, 湖南 长沙 410208, 中国

【摘要】目的 研究青光安 II 号方（QGA II）对慢性高眼压模型小鼠肠道菌群的影响，挖掘其保护视神经的关键菌群。**方法** 将 10 只无特定病原体（SPF）级 DBA/2J 雌性小鼠随机分成模型组、QGA II 组（每组 5 只），另取 5 只 SPF 级 C57BL/6J 雌性小鼠作为对照组。小鼠为自发型高眼压模型鼠，约从 7 月龄开始出现眼压升高。维持高眼压状态至 38 周龄开始灌胃，模型组和对照组给予等体积蒸馏水灌胃，QGA II 组给予 9.67 g/kg QGA II 灌胃，连续 4 周，每日 1 次。采用苏木精-伊红（HE）染色检查视网膜形态学，并对视网膜神经节细胞（RGCs）进行计数。免疫荧光法检测 RGCs 特异性标志物 Brn3a 蛋白的表达水平，测定平均光密度（OD）进行定量分析。同时用 16S rDNA 测序技术分析肠道菌群多样性，包括 α-多样性指数（Chao1 指数、Shannon 指数、Pielou 均匀度指数、观测物种指数）和 β-多样性指数变化情况，通过韦恩图和线性判别分析效应值（LEfSe）分析探究在门水平和属水平上各组小鼠肠道菌群的扩增子序列变异（ASVs）数量、差异物种丰度与差异物种分类。**结果** HE 染色显示，与对照组比较，模型组 RGCs 数量明显减少（$P < 0.01$），细胞内空泡变性、核固缩。QGA II 治疗后，小鼠 RGCs 数量较模型组显著增加（$P < 0.01$），细胞内空泡变性明显改善。免疫荧光分析显示，模型组小鼠 Brn3a 蛋白的平均 OD 较对照组显著降低（$P < 0.01$），而 QGA II 处理小鼠 Brn3a 蛋白的表达水平显著升高（$P < 0.01$）。α-多样性分析显示，QGA II 干预后，Chao1、Shannon 和 Pielou 均匀度指数显著升高（$P < 0.01$），观测物种指数显著升高（$P < 0.05$）。β-多样性分析显示，三组间存在明显的聚类，表明细菌群落结构相似性较低。ASVs 聚类在所有组中确定了 14 061 个 ASVs，其中 9 514 个 ASVs 在模型和 QGA II 组之间共享。在门水平上，与对照组相比，模型组拟杆菌门丰度显著降低（$P < 0.01$），厚壁菌门丰度和厚壁菌门/拟杆菌门（F/B）比值显著升高（$P < 0.01$）。QGA II 处理显著降低了厚壁菌门丰度和 F/B 比值（$P < 0.01$）。在属水平上，各组均以乳酸菌为优势菌，与对照组相比，模型组乳酸菌丰度显著升高（$P < 0.01$），QGA II 干预后其丰度降低（$P < 0.05$）。**结论** QGA II 可影响 DBA/2J 小鼠的肠道菌群结构，增加菌群多样性和丰富度，对厚壁菌门、拟杆菌门、乳杆菌属及其下属微生物的调节可能是 QGA II 发挥视神经保护作用的关键菌群。

【关键词】青光安 II 号方；慢性高眼压；16S rDNA 测序；视神经保护；肠道菌群